The maximum and minimum gain can be found by differentiating (13) with respect to X_{33}. The resulting quadratic equation

$$X_{33}^2(-M_bM_cX_{21}^2 - M_b^2X_{23}X_{31}X_{21}) - X_{33}[-M_dX_{21}^2 + (M_bX_{23}X_{31})^2 + (M_bR_sX_{21})^2] + M_dX_{23}X_{31}X_{21} + M_cM_b(X_{23}X_{31})^2 + M_bM_c(R_sX_{21})^2 = 0 \quad (14)$$

can be easily solved to find the desired gain extrema. In this equation $M_d = M_a + M_c^2$.

Appendix II

The midband gain sensitivity to variations in pump power given in (6) and (7) is obtained from the gain expression (5) where $S_2 = 0$. The factors used in (7) are

$$M_e = (R_g + R_s)(R_l + R_s) - S_1^2/(\omega_{10}\omega_{20})$$

$$M_f = (R_g + R_s)(R_l + R_s)R_s + (R_l + R_s)S_1^2/(\omega_{10}\omega_{30}) - R_sS_1^2/(\omega_{10}\omega_{20})$$

$$M_g = R_s - (R_l + R_s)\omega_{20}/\omega_{30}.$$

Appendix III

The parameters for the noise figure given in (10) are

$$M_x = \left(1 + \frac{R_s}{R_g}\right) X_{12}X_{21}R_s^2 + \frac{R_s}{R_g}[X_{23}^2(R_g + R_s)^2 + (X_{21}X_{13})^2 + X_{13}X_{31}X_{12}X_{21}] + \left(1 + \frac{R_s}{R_g}\right) \cdot [X_{23}X_{32}R_s(R_g + R_s) + X_{23}X_{32}X_{13}X_{31}] + \{[(R_g + R_s)(R_l + R_s)R_s - (R_g + R_s)X_{23}X_{32} + (R_l + R_s)X_{13}X_{31} + R_sX_{12}X_{21}]^2 + [X_{21}X_{13}X_{32} + X_{23}X_{31}X_{12}]^2\}/(4R_lR_g)$$

$$M_y = \left(1 + \frac{R_s}{R_g}\right)(X_{12}X_{23}X_{31} + X_{21}X_{13}X_{32}) - 2(X_{21}X_{13}X_{32} + X_{23}X_{31}X_{12})[(R_g + R_s)(R_l + R_s) - X_{12}X_{21}]/(4R_gR_l)$$

$$M_z = \left(1 + \frac{R_s}{R_g}\right) X_{12}X_{21} + [(R_g + R_s)(R_l + R_s) - X_{12}X_{21}]^2/(4R_gR_l).$$

Differentiating (10) with respect to X_{33} results in the following quadratic equation in X_{33}:

$$0 = X_{33}^2[-M_yX_{21}^2 + 2M_zX_{31}X_{23}X_{21}] + X_{33}[2M_z(X_{31}X_{23})^2 + 2M_z(X_{21}R_s)^2 - 2M_xX_{21}^2] + [M_y(X_{31}X_{23})^2 + M_y(X_{21}R_s)^2 - 2M_xX_{21}X_{31}X_{23}]$$

which can be easily solved to obtain the noise figure extrema.

References

[1] P. J. Khan, "Optimum design of low-noise lower sideband parametric up-converters," *IEEE Trans. Electron Devices*, vol. ED-18, pp. 924–931, Oct. 1971.

[2] J. A. Luksch, E. W. Matthews, and G. A. VerWys, "Design and operation of four-frequency parametric up-converters," *IRE Trans. Microwave Theory Tech.*, vol. MTT-9, pp. 44–52, Jan. 1961.

[3] D. B. Anderson and J. C. Aukland, "Transmission-phase relations of four-frequency parametric devices," *IRE Trans. Microwave Theory Tech.*, vol. MTT-9, pp. 491–498, Nov. 1961.

[4] A. Korpel and V. Ramaswamy, "Input conductance of four-frequency parametric up-converter," *IEEE Trans. Microwave Theory Tech.*, vol. MTT-13, pp. 96–106, Jan. 1965.

[5] R. L. Ernst, "Multiple-idler parametric amplifiers," *IEEE Trans. Microwave Theory Tech.*, vol. MTT-15, pp. 9–22, Jan. 1967.

[6] D. P. Howson and R. B. Smith, *Parametric Amplifiers*. London, England: McGraw-Hill, 1970, ch. 6.

[7] B. J. Robinson, "Theory of variable-capacitance parametric amplifiers," *Proc. Inst. Elec. Eng.*, Mono 480E, Nov. 1961.

[8] P. J. Khan, "Parametric amplifier nonresonant gain maximum," *Proc. IEEE* (Lett.), vol. 56, pp. 99–100, Jan. 1968.

[9] K. Kurokawa, "Actual noise measure of linear amplifiers," *Proc. IRE*, vol. 49, pp. 1391–1397, Sept. 1961.

General Field Theory Treatment of *H*-Plane Waveguide Junction Circulators

M. EZZAT EL-SHANDWILY, AHMAD A. KAMAL, AND ESMAT A. F. ABDALLAH

Abstract—**In this paper an exact field theory treatment for the waveguide junction circulators is presented. The treatment is general, being dependent on neither the geometrical symmetry of the junction nor the number of ports. The electromagnetic fields in the joining waveguides are written in the form of infinite summation of waveguide modes. The solutions of the wave equations in the ferrite rod and in the surrounding air are obtained in the form of infinite summation of cylindrical modes. The fields at the ferrite air interface and at an imaginary boundary chosen arbitrarily between the air region and the waveguides are then matched. This process leads to an infinite system of nonhomogeneous equations in the field amplitudes.**

Three types of waveguide junction circulators using this technique are analyzed: the simple ferrite-rod Y junction, the simple ferrite-rod T junction, and the latching Y junction.

Point-matching techniques are used to get numerical results for the field distributions and the circulator characteristics. Excellent agreement has been found between the published experimental measurements and the numerical results obtained by this technique.

Manuscript received August 25, 1972; revised December 13, 1972.

M. E. El-Shandwily and E. A. F. Abdallah are with the Electrical and Electronic Engineering Laboratory, National Research Centre, Dokki, Cairo, Egypt.

A. A. Kamal is with the Department of Electronic and Communication Engineering, Faculty of Engineering, Cairo University, Cairo, Egypt.

I. Introduction

AFTER a comprehensive study of junction circulators, it has been found that the only theoretical treatment that exists for the waveguide junction circulator is that of Davies [1]. In his analysis for a symmetrical N-port junction circulator he made use of the properties of the scattering matrix and its eigenvalues. Expressions for these eigenvalues in terms of the fields inside the junction are obtained. This analysis, however, is limited for junctions that have geometrical symmetry. Also Davies in his numerical computations considered only the dominant mode in the waveguide and the center region. This neglect of the higher modes is the reason for the discrepancy between the numerical results and the experimental measurements obtained by Davis and Castillo [2], [3]. This deviation is particularly manifested in the value of circulation frequency, the isolation at this frequency, as well as the general shape of the reflection coefficient curve. The limitations in the analysis by Davies stimulated this paper, in which an exact field theory treatment for the waveguide junction circulator is presented. The treatment is general in such a way that it depends on neither the geometrical symmetry of the junction nor the number of ports.

The circulator consists of N waveguides intersecting as shown schematically in Fig. 1. The ferrite rod is placed inside the junction and the dc magnetic field is applied normal to the plane of the junction. In general, the waveguides need not be symmetrically located around the junction. The system is assumed to be free of any losses and excitation by the dominant mode TE_{10} as only one of the waveguides takes place. It is further assumed that the output ports are perfectly matched, and the electromagnetic-field components have a time dependence in the form exp $(j\omega t)$. Since the ferrite cylinder is assumed smooth, in the plane of the junction, the scattered electric fields will be normal to the plane of the junction. Therefore, only TE_{m0} modes are excited such that the boundary conditions at the greater sides of the waveguides are always satisfied. The waveguides are assumed to propagate only the dominant TE_{10} mode, while all higher modes are cut off.

Matching of the fields takes place at the ferrite–air interface and at the common boundaries between the junction and the waveguides. Thus it is possible to obtain the magnitude and the phase of the electromagnetic-field components at each point within the junction. By this technique, one can obtain the circulator characteristics (reflection coefficient, isolation, and insertion loss) for different operating conditions (ferrite radius, applied dc magnetic field, saturation magnetization, etc.).

This technique is applied to the two symmetrical circulators, namely the simple rod Y junction and the latching Y junction. Since this treatment is general and does not depend on the symmetry of the junction, it is applied to the T junction, which does not have the same rotational symmetry.

II. Theoretical Analysis of N-Port Circulators

The junction may be considered as divided into three regions, the ferrite rod, the surrounding air region, and the waveguides as shown in Fig. 1. The electric field Ey in the ferrite rod (region I) satisfies the homogeneous Helmholtz equation:

$$\nabla_t^2 Ey + k_f^2 Ey = 0 \tag{1}$$

where

∇_t^2 the Laplacian operator in the plane of the junction;
k_f^2 $= \omega^2 \mu_0 \epsilon_0 \mu_{eff} \epsilon_f$;

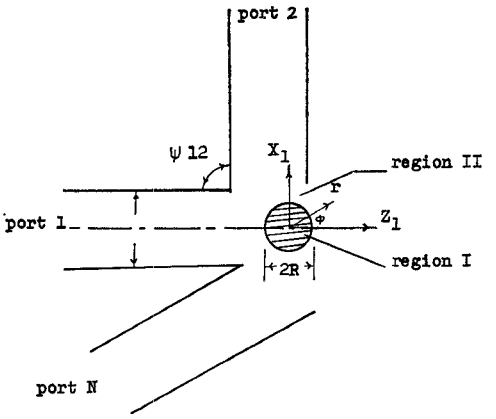

Fig. 1. Schematic representation of N-port nonsymmetrical waveguide junction circulator.

$$\mu_{eff} = \frac{\mu^2 - k^2}{\mu},$$

μ, k diagonal and off-diagonal permeability tensor components;
ϵ_f relative permittivity of ferrite material.

The solution of (1) takes the following form:

$$Ey(r, \phi) = \sum_{n=0}^{\infty} J_n(k_f r)[a_n \cos(n\phi) + b_n \sin(n\phi)] \tag{2}$$

and from Maxwell's equations the azimuthal magnetic-field component is

$$H_\phi(r, \phi) = jY_f \sum_{n=0}^{\infty} \left\{ a_n \left[J_n'(k_f r) \cos(n\phi) - \frac{jnk}{\mu k_f r} J_n(k_f r) \sin(n\phi) \right] + b_n \left[J_n'(k_f r) \sin(n\phi) + \frac{jnk}{\mu k_f r} \cos(n\phi) \right] \right\} \tag{3}$$

where $Y_f = \sqrt{\epsilon_0 \epsilon_f / \mu_0 \mu_{eff}}$ is the wave admittance in the ferrite. The dash denotes differentiation with respect to the argument, and a_n and b_n are constants. The electric-field component in the air region surrounding the ferrite post (region II) also satisfies the wave equation:

$$\nabla_t^2 Ey + k_0^2 Ey = 0 \tag{4}$$

where

$$k_0^2 = \omega^2 \mu_0 \epsilon_0.$$

The solution of (4) is

$$Ey(r, \phi) = \sum_{n=0}^{\infty} \{ J_n(k_0 r)[d_n \cos(n\phi) + g_n \sin(n\phi)] + Y_n(k_0 r)[e_n \cos(n\phi) + f_n \sin(n\phi)] \} \tag{5}$$

and the azimuthal magnetic field is

$$H_\phi(r, \phi) = -jY_a \sum_{n=0}^{\infty} \{ J_n'(k_0 r)[d_n \cos(n\phi) + g_n \sin(n\phi)] + Y_n'(k_0 r)[e_n \cos(n\phi) + f_n \sin(n\phi)] \} \tag{6}$$

where $Y_a = \sqrt{\epsilon_0/\mu_0}$ and d_n, g_n, e_n, and f_n are constants. The incident electromagnetic-field components in waveguide 1 are given by

$$Ey^{\text{in}}(x_1, z_1) = \sin\left[\frac{(1 + 2x_1/a)\pi}{2}\right] e^{-jk_1 z_1} \tag{7}$$

$$H_x^{\text{in}}(x_1, z_1) = \frac{-k_1}{\omega\mu_0} \sin\left[\frac{(1 + 2x_1/a)\pi}{2}\right] e^{-jk_1 z_1} \tag{8}$$

$$H_z^{\text{in}}(x_1, z_1) = \frac{j\gamma_1}{\omega\mu_0} \cos\left[\frac{(1 + 2x_1/a)\pi}{2}\right] e^{-jk_1 z_1} \tag{9}$$

where

a = waveguide width
$k_1 = \sqrt{k_0^2 - \gamma_1^2}$
$\gamma_1 = \pi/a$.

The junction and the ferrite post present a discontinuity to the incident field, and therefore scattered fields are induced in all waveguides. The scattered field in waveguide 1 represents the reflected wave. In general the scattered field in the ith waveguide can be written as

$$E_y^i(x_i, z_i) = \sum_{m=1}^{\infty} A_m^i \sin\left[\frac{(1 + 2x_i/a)m\pi}{2}\right] e^{jk_m z_i} \tag{10}$$

$$H_x^i(x_i, z_i) = \frac{1}{\omega\mu_0} \sum_{m=1}^{\infty} A_m^i k_m \sin\left[\frac{(1 + 2x_i/a)m\pi}{2}\right] \cdot e^{jk_m z_i} \tag{11}$$

$$H_z(x_i, z_i) = \frac{j}{\omega\mu_0} \sum_{m=1}^{\infty} A_m^i \gamma_m \cos\left[\frac{(1 + 2x_i^2/a)m\pi}{2}\right] \cdot e^{jk_m z_i} \tag{12}$$

where

γ_m $= m\pi/a, \quad m = 1, 2, 3, \cdots$;
k_m $= -j\sqrt{\gamma_m^2 - k_0^2}$;
A_1^1 complex reflection coefficient at the input port;
A_1^i complex transmission coefficient to the ith port;
$A_2^i, A_3^i, \cdots$ complex amplitudes of the evanscent modes in the ith waveguide;
x_i, z_i rectangular coordinates in waveguide i, which are obtained by rotating the system of axes (x_1, z_1) by an angle ψ_{1i}, as shown in Fig. 1, in the negative direction of ϕ.

The different constants in (2)–(12), namely a_n, d_n, g_n, e_n, f_n, and A_m^i can be obtained from the continuity conditions of the tangential field components at the ferrite–air interface and at an imaginary boundary joining the air region and each waveguide. These boundary conditions are

$$E_y(R, \phi)\big|_{\text{ferrite}} = E_y(R, \phi)\big|_{\text{air}}, \qquad 0 \le \phi \le 2\pi \tag{13}$$

$$H_\phi(R, \phi)\big|_{\text{ferrite}} = H_\phi(R, \phi)\big|_{\text{air}}, \qquad 0 \le \phi \le 2\pi. \tag{14}$$

From these two equations, (2) and (6), and the orthogonality properties of the trigonometric functions, we get

$$\begin{aligned} d_n &= M_{1n}a_n + jM_{2n}b_n \\ e_n &= M_{3n}a_n + jM_{4n}b_n \\ f_n &= -jM_{4n}a_n + M_{3n}b_n \\ g_n &= -jM_{2n}a_n + M_{1n}b_n \end{aligned} \tag{15}$$

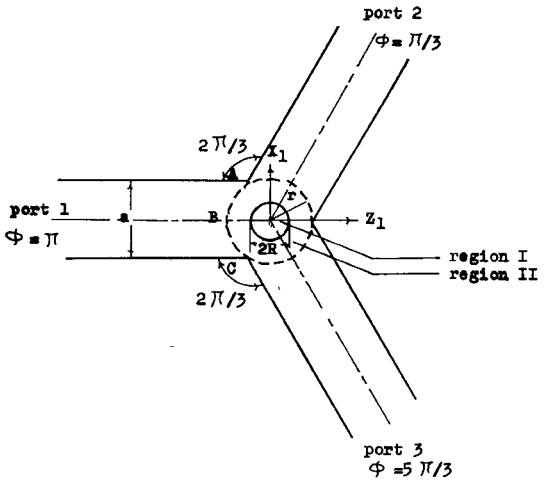

Fig. 2. Schematic representation of Y-junction circulator.

where

$$M_{1n} = \frac{-\pi k_0 R}{2}\left[\frac{Y_f}{Y_a} Y_n(k_0R)J_n'(k_fR) - Y_n'(k_0R)J_n(k_fR)\right]$$

$$M_{2n} = \frac{-\pi k_0 R}{2}\left[\frac{nk}{\mu k_f R}\cdot\frac{Y_f}{Y_a}\cdot J_n(k_fR)\, Y_n(k_0R)\right]$$

$$M_{3n} = \frac{\pi k_0 R}{2}\left[\frac{Y_f}{Y_a} J_n(k_0R)J_n'(k_fR) - J_n(k_fR)J_n'(k_0R)\right]$$

$$M_{4n} = \frac{\pi k_0 R}{2}\left[\frac{nk}{\mu k_f R}\cdot\frac{Y_f}{Y_a}\cdot J_n(k_0R)J_n(k_fR)\right].$$

The boundary conditions on the imaginary walls, between the air surrounding the ferrite post and the waveguides, depend on the geometry of the junction. In what follows, each of the junctions is thus treated separately and only the 3-port circulators are considered.

A. The Simple Rod Y-Junction Circulator

The waveguide field expressions in port 1 are valid up to the straight line AC, and the circular field expressions (region II) are valid up to the arc ABC. According to the discussion given by Lewin and Nielsen [4] and Lewin [5] any boundary in the meniscus region ABC can be used for matching the fields.

The imaginary wall in this case is chosen to be a cylindrical wall whose axis coincides with the junction axis. From the geometry shown in Fig. 2, it follows that the radius of the imaginary wall is $a/\sqrt{3}$. The boundary conditions on this wall are for the ith waveguide:

$$E_y(r, \phi)\big|_{\text{air}} = E_y(x_i, z_i)\big|_{\text{waveguide } i} \tag{16}$$

$$H_\phi(r, \phi)\big|_{\text{air}} = -H_z(x_i, z_i)\sin\phi_i + H_x(x_i, z_i)\cos\phi_i \tag{17}$$

where

$$\begin{aligned} i &= 1, 2, 3 \\ r &= a/\sqrt{3} \\ x_i &= a\sin\phi_i/\sqrt{3} \end{aligned}$$

$$z_i = a \cos \phi_i/\sqrt{3}$$

$$\phi_i = \phi + (i-1)\frac{2\pi}{3}, \qquad \frac{2\pi}{3} \leq \phi_i \leq \frac{4\pi}{3}.$$

Using the previous field expressions together with (16) and (17), the following set of nonhomogeneous equations in the infinite unknowns $A_m{}^i$, a_n, and b_n are obtained:

$$\sum_{m=1}^{\infty} A_m{}^i \sin\left[\frac{(1+2\sin\phi_i/\sqrt{3})m\pi}{2}\right] e^{jak_m \cos\phi_i/\sqrt{3}}$$

$$-\sum_{n=0}^{\infty} a_n \left\{\cos(n\phi)\cdot\left[J_n\left(\frac{ak_0}{\sqrt{3}}\right)M_{1n} + Y_n\left(\frac{ak_0}{\sqrt{3}}\right)M_{3n}\right]\right.$$

$$\left.-j\sin(n\phi)\left[J_n\left(\frac{ak_0}{\sqrt{3}}\right)M_{2n} + Y_n\left(\frac{ak_0}{\sqrt{3}}\right)M_{4n}\right]\right\}$$

$$-\sum_{n=0}^{\infty} b_n \left\{j\cos(n\phi)\cdot\left[J_n\left(\frac{ak_0}{\sqrt{3}}\right)M_{2n} + Y_n\left(\frac{ak_0}{\sqrt{3}}\right)M_{4n}\right]\right.$$

$$\left.+\sin(n\phi)\left[J_n\left(\frac{ak_0}{\sqrt{3}}\right)M_{1n} + Y_n\left(\frac{ak_0}{\sqrt{3}}\right)M_{3n}\right]\right\}$$

$$= -\delta_{1i}\sin\left[\frac{(1+2\sin\phi_i/\sqrt{3})\pi}{2}\right] e^{-jak_1\cos\phi_i/\sqrt{3}} \tag{18}$$

$$-\frac{j\sin\phi_i}{\omega\mu_0}\sum_{m=1}^{\infty} A_m{}^i\gamma_m \cos\left[\frac{(1+2\sin\phi_i/\sqrt{3})m\pi}{2}\right]$$

$$\cdot e^{jak_m\cos\phi_i/\sqrt{3}} + \frac{\cos\phi_i}{\omega\mu_0}\sum_{m=1}^{\infty} A_m{}^i k_m$$

$$\cdot\sin\left[\frac{(1+2\sin\phi_i/\sqrt{3})m\pi}{2}\right] e^{jak_m\cos\phi_i/\sqrt{3}}$$

$$+jY_a\sum_{n=0}^{\infty} a_n\left\{\cos(n\phi)\left[J_n'\left(\frac{ak_0}{\sqrt{3}}\right)M_{1n}\right.\right.$$

$$\left.+Y_n'\left(\frac{ak_0}{\sqrt{3}}\right)M_{3n}\right] - j\sin(n\phi)\left[J_n'\left(\frac{ak_0}{\sqrt{3}}\right)M_{2n}\right.$$

$$\left.\left.+Y_n'\left(\frac{ak_0}{\sqrt{3}}\right)M_{4n}\right]\right\} + jY_a\sum_{n=0}^{\infty} b_n\left\{j\cos(n\phi)\right.$$

$$\cdot\left[J_n'\left(\frac{ak_0}{\sqrt{3}}\right)M_{2n} + Y_n'\left(\frac{ak_0}{\sqrt{3}}\right)M_{4n}\right]$$

$$\left.+\sin(n\phi)\left[J_n'\left(\frac{ak_0}{\sqrt{3}}\right)M_{1n} + Y_n'\left(\frac{ak_0}{\sqrt{3}}\right)M_{3n}\right]\right\}$$

$$= \delta_{1i}\left\{\frac{j\gamma_1\sin\phi_i}{\omega\mu_0}\cos\left[\frac{(1+2\sin\phi_i/\sqrt{3})\pi}{2}\right] e^{-jak_1\cos\phi_i/\sqrt{3}}\right.$$

$$\left.+\frac{k_1\cos\phi_i}{\omega\mu_0}\sin\left[\frac{(1+2\sin\phi_i/\sqrt{3})\pi}{2}\right] e^{-jak_1\cos\phi_i/\sqrt{3}}\right\} \tag{19}$$

where δ_{1i} is the Kronecker delta.

It is to be noted that since $i=1$, 2, and 3, (18) and (19) represent six nonhomogeneous equations. Since the unknowns involved in these equations are infinite, an infinite number of equations is required to obtain an exact solution. In this problem as in most problems solved by modal methods, a closed-form exact solution is not possible. However, results to any degree of accuracy can be obtained by taking a sufficient number of waveguide and cylindrical modes into account.

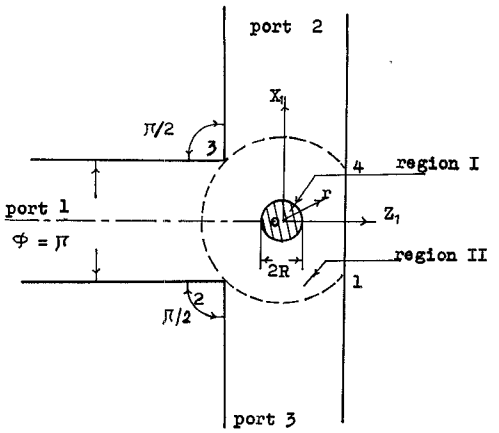

Fig. 3. Schematic representation of T-junction circulator.

Consider m waveguide modes and n cylindrical modes; the number of unknowns is $(3m+2n+1)$. The application of (18) and (19) at one point on the boundary between each waveguide and the air region gives six equations in the unknowns. However, for q matching points in each waveguide, the number of equations is $6q$. For the number of equations to be equal to the number of unknowns it is necessary to have

$$6q = 3m + 2n + 1. \tag{20}$$

It should be noted that for any value of q, the values of m and n that satisfy (20) are not unique.

B. The T-Junction Circulator

The boundary selected for matching the fields of the air surrounding the ferrite post and the waveguides is a cylindrical wall of radius $a/\sqrt{2}$ as shown in Fig. 3. Another condition that should be satisfied, in this case, is that the electric field $Ey(r, \phi)$ of region II has a zero value on the metallic wall 1–4 in Fig. 3. It should be noted that this is a valid boundary for matching the fields since the first singularity in the expansion of the cylindrical fields in region II appears at a distance a from the origin and our chosen boundary is inside this region [4]. The boundary condition can thus be written as follows.

For the ith waveguide:

$$Ey(r,\phi)\,|_{\text{air}} = Ey(x_i, z_i)\,|_{\text{waveguide } i} \tag{21}$$

$$H_\phi(r,\phi)\,|_{\text{air}} = -H_z(x_i, z_i)\sin\phi_i + H_x(x_i, z_i)\cos\phi_i\,|_{\text{waveguide } i} \tag{22}$$

where

$$i = 1, 2, 3$$

$$r = a/\sqrt{2}$$

$$x_i = a\sin\phi_i/\sqrt{2}$$

$$z_i = a\cos\phi_i/\sqrt{2}$$

$$\phi_1 = \phi, \qquad 3\pi/4 \leq \phi \leq 5\pi/4$$

$$\phi_2 = \phi + \pi/2, \qquad \pi/4 \leq \phi \leq 3\pi/4$$

$$\phi_3 = \phi + 3\pi/2, \qquad 5\pi/4 \leq \phi \leq 7\pi/4;$$

For region II:

$$Ey(r,\phi)\,|_{\text{air}} = 0 \tag{23}$$

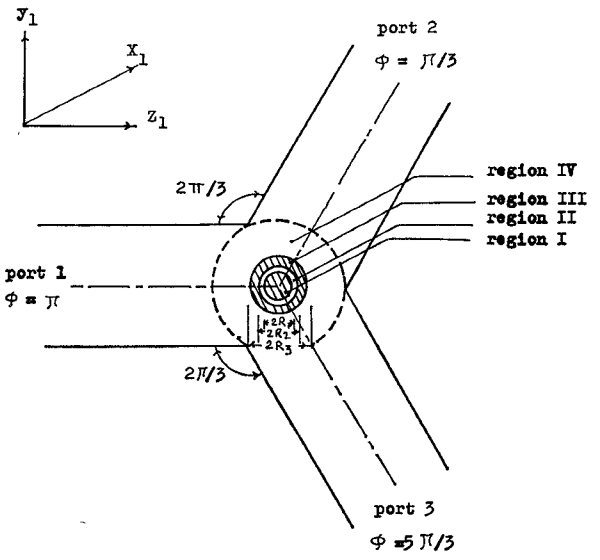

Fig. 4. Schematic representation of Y-junction latching circulator.

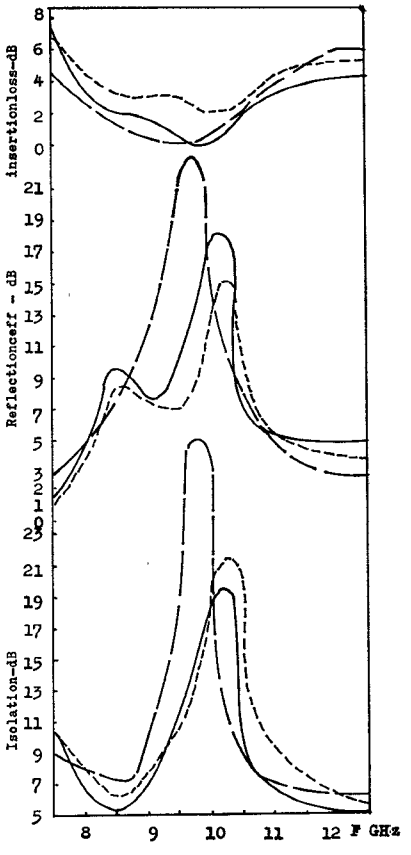

Fig. 5. Circulator characteristics for Y-junction circulator, using sample TT2-130, $R=0.35$ cm and $H_{in}=200$ Oe. —— Point by point. ----- Experimental. —— —— Davis and Castillo.

where

$$r = \frac{a}{2\cos\phi}, \qquad 7\pi/4 \leq \phi \leq \pi/4.$$

The first two of these three equations are similar to those obtained for the Y-junction circulator. The additional equation

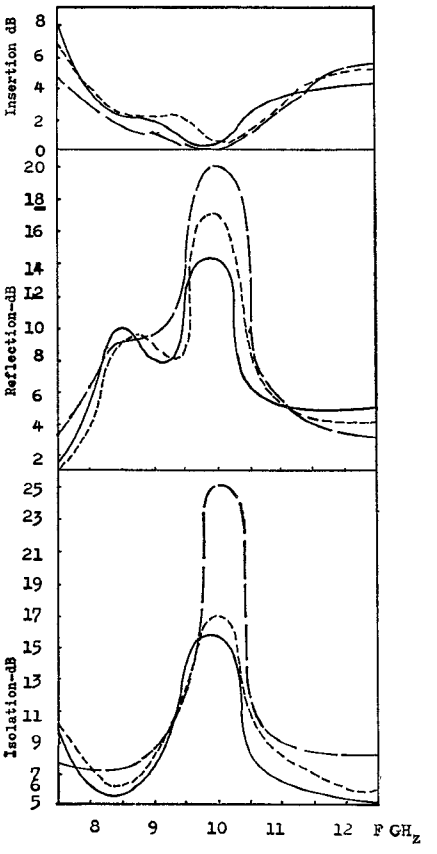

Fig. 6. Circulator characteristics for Y-junction circulator, using sample TT1-109, $R=0.35$ cm and $H_{in}=200$ Oe. —— Point by point. ----- Experimental. —— —— Davis and Castillo.

(23) results from the additional condition imposed on the boundary 1–4 in Fig. 3.

For m waveguide modes and n cylindrical modes, the number of unknowns is still the same as before $(3m+2n+1)$. Hence taking q matching points in each waveguide and l points on the conducting boundary, the number of equations is given by $(6q+l)$. This number of equations should equal the number of unknowns, thus

$$6q + l = 3m + 2n + 1. \tag{24}$$

III. Theoretical Analysis of Y-Junction Latching Circulator

The stripline latching circulator has been analyzed by Siekanowicz and Schilling [6]. The analysis of the waveguide latching circulator shown in Fig. 4 is presented in this section using the same technique as for the unidirectionally magnetized Y-junction circulators. The junction in this case, however, is divided into five regions, namely the ferrite rod, the nonmagnetic gap, the ferrite cylinder, the air region, and the waveguides, as shown in Fig. 4. The field components in the different regions are written as before in terms of infinite summations over Bessel's functions with arbitrary constants to be determined from the matching conditions at the boundaries. These boundary conditions are the equality of the tangential electric- and magnetic-field components at R_1, R_2, and R_3.

The boundary conditions on the imaginary walls between the air regions and the waveguides are specified as in the unidirectional circulators. The relation (20) between the number

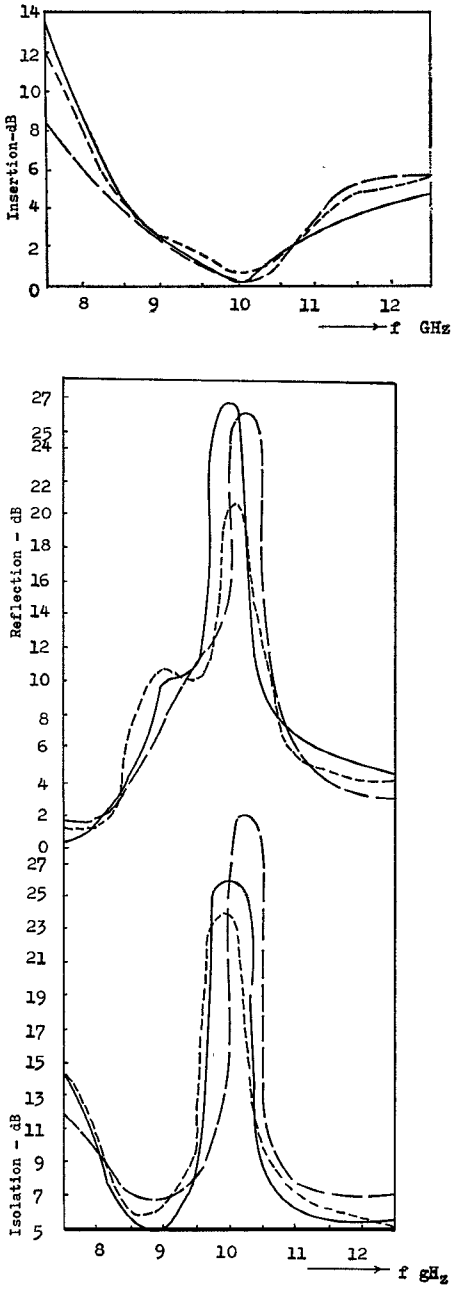

Fig. 7. Circulator characteristics for Y-junction circulator, using sample G-1002, $R = 0.3$ cm, and $H_{in} = 200$ Oe.

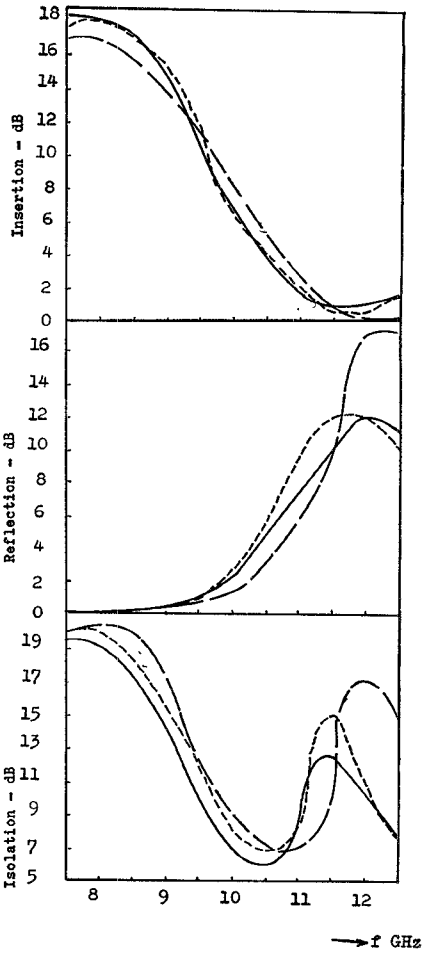

Fig. 8. Circulator characteristics for Y-junction circulator, using sample G-1002, $R = 0.25$ cm and $H_{in} = 200$ Oe. ——— Point by point. ----- Experimental. —— —— Davis and Castillo.

of matching points and the number of cylindrical and waveguide modes is also valid in this case.

The six nonhomogeneous equations obtained in the case of unidirectional and latching Y circulators, and also the seven equations obtained in the case of T junction are exact. Thus with an infinite number of matching points between the air region and the waveguides an exact field distribution within the junction is known. In the next section, only a finite number of matching points is used to solve the equations by numerical techniques.

IV. Numerical Results and Discussions

In this section numerical techniques are used to solve the equations derived in the previous section for the different types of circulators. With a finite number of matching points chosen for each type of junction, a finite number of simultaneous nonhomogeneous equations are solved together with the aid of a digital computer. The truncation of the infinite series in the simultaneous equations amounts to taking only a finite number of waveguide modes and cylindrical modes, on the assumption that the neglected modes have much smaller amplitudes. It should be noted that the point-matching technique has been used recently in solving the problem of propagation in waveguides with arbitrary cross sections and scattering from metallic boundaries of arbitrary shapes [7]–[9].

The two conditions to indicate the accuracy of the results are as follows.

1) The output power from the three ports, i.e., the summation of the reflected power from the input port and the output power from the other two ports, should equal the incident power, from which we get

$$\sum_i |A_1^i|^2 = 1. \tag{25}$$

2) The rapidity of the convergence of the infinite series representing the fields. This can be indicated by taking a number of matching points and obtaining the mode amplitudes, then increasing the matching points and noting the change in the mode amplitudes previously calculated. When the change is insignificant, then the original matching points are considered to be sufficient.

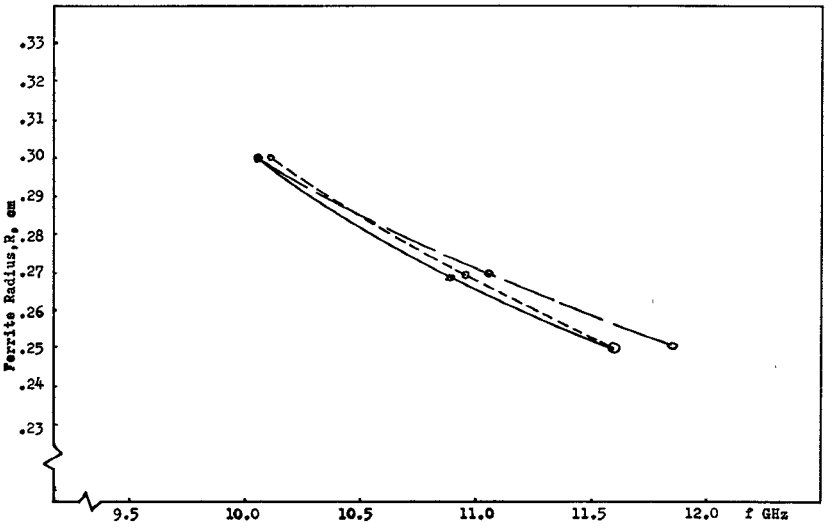

Fig. 9. Frequency of best isolation versus ferrite radius. —— Point by point. ----- Experimental. —— —— Davis and Castillo.

A. Numerical Results of Simple Rod Y-Junction Circulator

The cases of one, three, and five matching points on the imaginary boundary in each waveguide are considered. Accordingly, one, three, and five waveguide modes and two, six, and eight cylindrical modes are retained, respectively. In all three cases the power condition, (25), is satisfied to an accuracy of $\pm 10^{-6}$. However, the lowest order waveguide and cylindrical modes varied considerably when taking $q=1$ and 3, while the difference between these modes in the cases of $q=3$ and 5 is small, especially when converted to decibels. This difference is in the order of 0.1 dB. This insignificant difference does not deserve the much increased computer time (three times the case of $q=3$). Therefore, three matching points in each waveguide are taken in the following numerical results.

The numerical solution of the Y-junction circulator is divided into two parts: the first considers the circulator characteristics while the second part considers the field- and power-density distributions inside the junction.

1) Circulator Characteristics: Numerical results are obtained for four different ferrite samples. The internal dc magnetic field H_{in} used in all the calculations is 200 Oe. The circulator characteristics using the four samples are shown in Figs. 5–8. The experimental results of Davis and Castillo [2], [3] and their theoretical calculations based on the analysis of Davies are also indicated in the same figures.

Fig. 5 shows the numerical results using sample TT2-130. The frequency of best isolation from Davis and Castillo's results is found to be 9.7 GHz theoretically, and 10.2 GHz experimentally. The corresponding result, based on the technique adopted in this paper, is 10.2 GHz, which is in agreement with the experimental measurements of Castillo and Davis. Their values for maximum isolation are -29 dB theoretically and -21.5 dB experimentally. The corresponding value determined by the adopted technique is -19.8 dB, which is much closer to the experimental value than the theoretical value of Davis and Castillo [1].

As has been noticed by Davis and Castillo, the most important difference between their experimental and theoretical results is in the general shape of the reflection coefficient, mainly in the frequency range from 8.5 GHz to 10.0 GHz. While the experimental measurements show double hump, their theoretical calculations show continuous decrease in the reflection coefficient. It is important to note that the adopted technique of analysis reveals the same double-hump behavior found experimentally. Also, while the theoretical reflection coefficient as determined by Davis and Castillo is about 8 dB smaller than their experimental prediction, that found in this study differs only by about 3 dB from the published experimental figure. It is therefore conclusive that for the ferrite sample TT2-130, results using the technique explained in the previous section are much closer to the experimental measurements than previously determined theoretical figures. Figs. 6–8 also show the same agreement with the experimental measurements.

The only parameters that can be changed with a particular ferrite material in a circulator are the applied magnetic field and the ferrite radius. While the internal dc magnetic field is kept constant at 200 Oe, the effect of the variation of the ferrite radius against the frequency of best isolation using sample G-1002 is shown in Fig. 9. The same figure also shows the corresponding theoretical and experimental results of Davis and Castillo. It is clear from the figure that as the radius decreases, the circulation frequency increases almost linearly. The figure also indicates that results obtained by the point-by-point matching technique fit the experimental measurements better than those obtained by the previous method of Davis and Castillo.

In a recent paper by Castillo and Davis [10], they extended their analysis to include the first two evanescent waveguide modes and up to the fifth cylindrical mode. The results obtained are in good agreement with the experimental measurements.

2) Field and Power Density Distributions: Once the constants $a_n, \cdots, f_n$ are known, the electromagnetic-field components at any point (r, ϕ) within the junction are determined. Figs. 10 and 11 show the electric-field distribution in the ferrite rod and the air ring for different values of the radius r as a parameter when using sample G-1002 at circulation frequency (11.6 GHz). These figures indicate that the electric field attains almost a minimum value at the isolated waveguide axis.

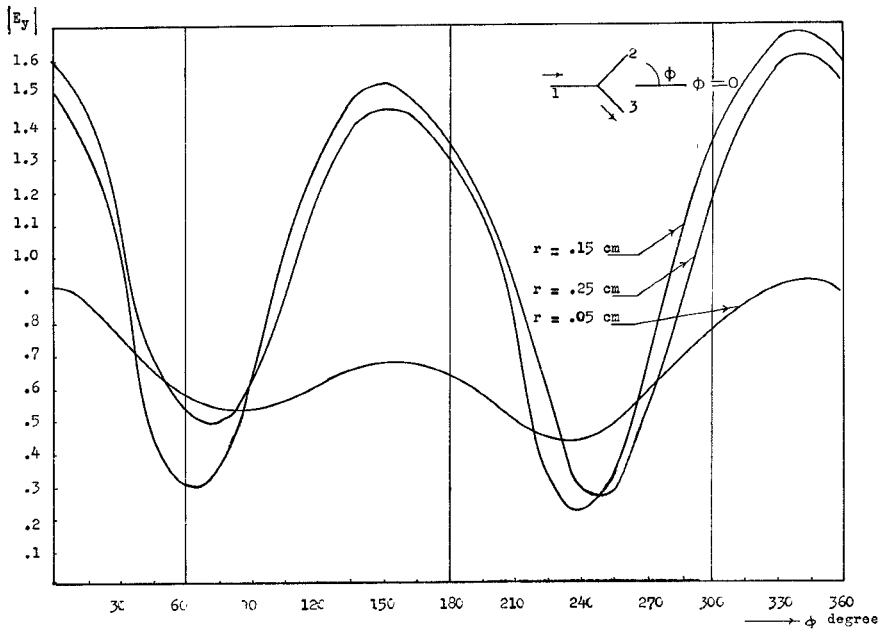

Fig. 10. Electric-field distribution in the ferrite rod using sample G-1002, $R=0.25$ cm and $H_{in}=200$ Oe.

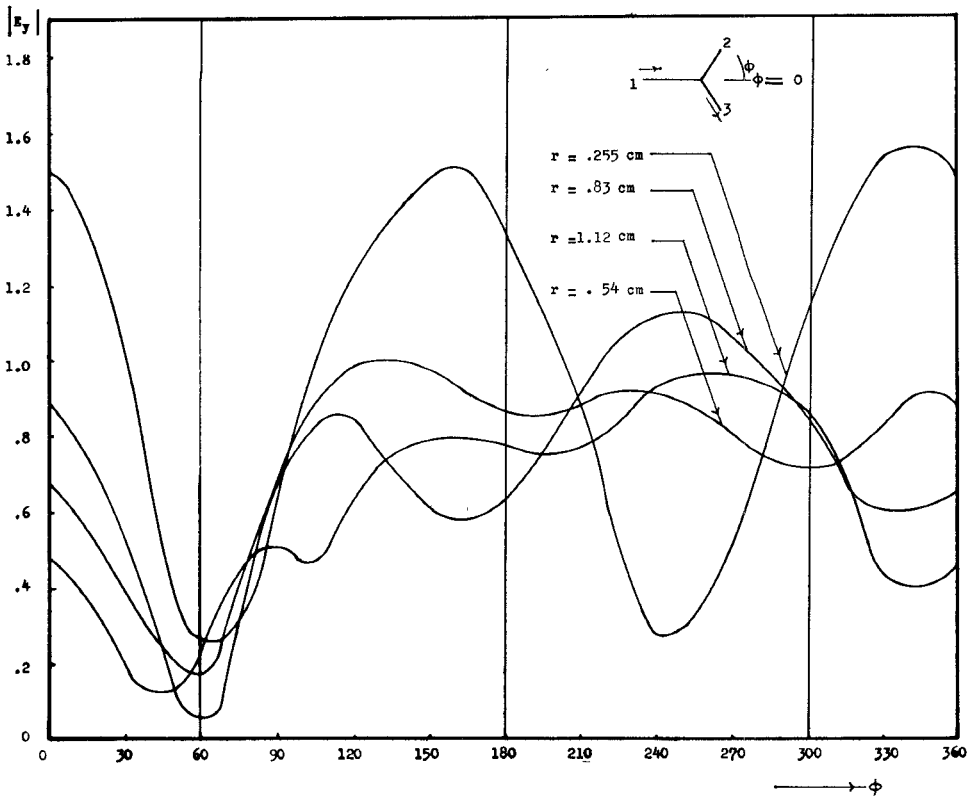

Fig. 11. Electric-field distribution in the air ring using sample G-1002, $R=0.25$ cm and $H_{in}=200$ Oe.

At the axes of the input and output ports the electric fields are approximately equal, although their phases are different. It should be noted that with an incident electric field of a maximum amplitude of unity, the amplitude of the electric field was found to attain higher values than unity at certain points inside the junction. The reason for this increase is that the fields inside the junction are due to both the incident and scattered fields; at some points they add inphase, while at other points they may subtract.

For the ferrite and air regions, the field distributions along the two arcs opposite to the input and output ports are approximately similar.

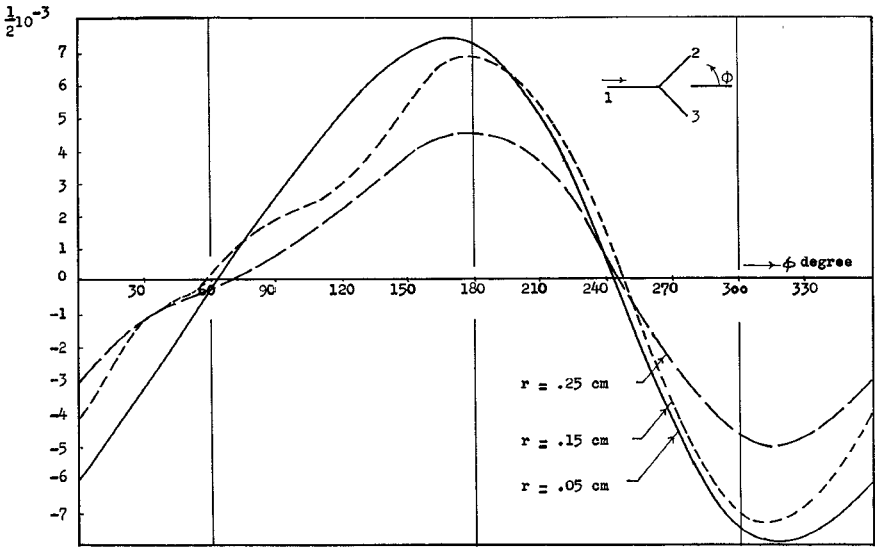

Fig. 12. Power-density distribution in the ferrite rod using sample G-1002, $R = 0.25$ cm and $H_{in} = 200$ Oe.

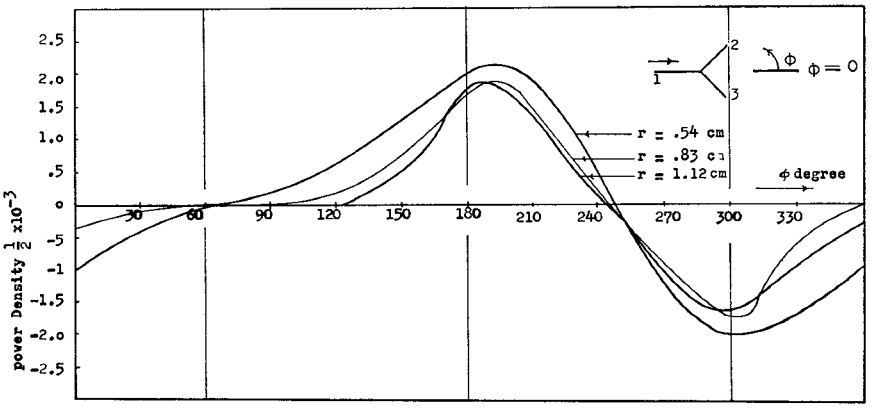

Fig. 13. Power-density distribution in the air ring using sample G-1002, $R = 0.25$ cm and $H_{in} = 200$ Oe.

From the electromagnetic-field components, the power-density flow in the radial direction is given by

$$p_r = \tfrac{1}{2} R_e(\overline{E} \times \overline{H}^*) \cdot \bar{a}_r \qquad (26)$$

where $\bar{a}_r$ is the unit vector in the radial direction. Figs. 12 and 13 show a plot of the power density distribution p_r in the ferrite rod and in the air ring, respectively, with the same values of r used to determine the field distribution. The power flow per unit height along an arc opposite to any waveguide is given by the area under the curve extending along that arc multiplied by the value of the arc radius. It is seen from Figs. 12 and 13 that for the isolated port (port 2), p_r is approximately zero along the axis, and it is of different signs in the two sides such that the total area under the curve extending along this port is approximately zero. For the arc opposite to the input port the power is always positive, while the power along the arc opposite to the output port (port 3) is negative, and the two areas are approximately equal. This difference in sign is due to the fact that the power in the input port is entering the junction, while the power in the output port is leaving the junction. It should be noted that as the radius increases the power density p_r decreases such that the area under the curve multiplied by the corresponding radius is constant.

B. Simple Rod T-Junction Circulator

In this case the characteristics of the junction as a circulator depend on which of the three ports is used as the input port.

1) Input from the Symmetrical Arm: The numerical results using sample TT2-130 are shown in Fig. 14. Comparing the results for this sample in the T and Y junction, shown in Figs. 14 and 5, respectively, the isolation characteristics have the same general shape. The frequency of best isolation for the T junction is shifted by about 0.3 GHz with respect to the Y junction. However, the isolation at this frequency for the Y junction is better by 6 dB. The general shape of the reflection coefficient for both junctions differs appreciably, and the T junction does not show the double hump encountered with the Y junction. It should be noted, however, that the insertion-loss curves in Y circulator are totally different. It can be seen that with T circulator another circulation frequency in the opposite direction takes place at 8.5 GHz. At this circulation frequency, better characteristics are obtained, namely higher isolation and smaller insertion loss with approximately the same value of reflection coefficient. This indicates that there are two circulation frequencies with opposite senses of circulation. The results using sample TT1-109, shown in

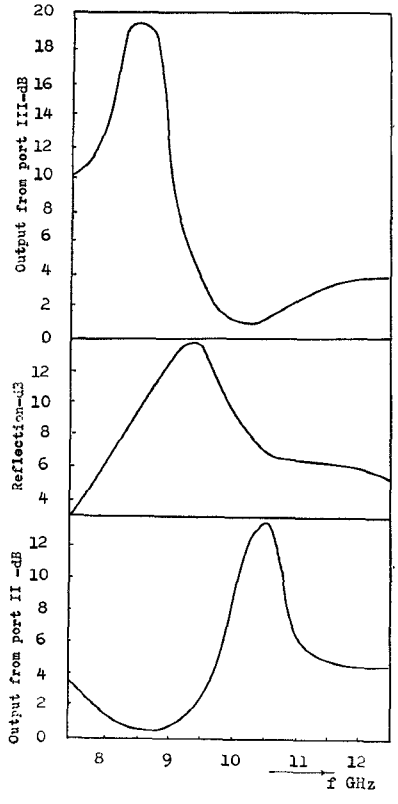

Fig. 14. Circulator characteristics for symmetrical T junction using sample TT2-130, $R=0.35$ cm and $H_{in}=200$ Oe.

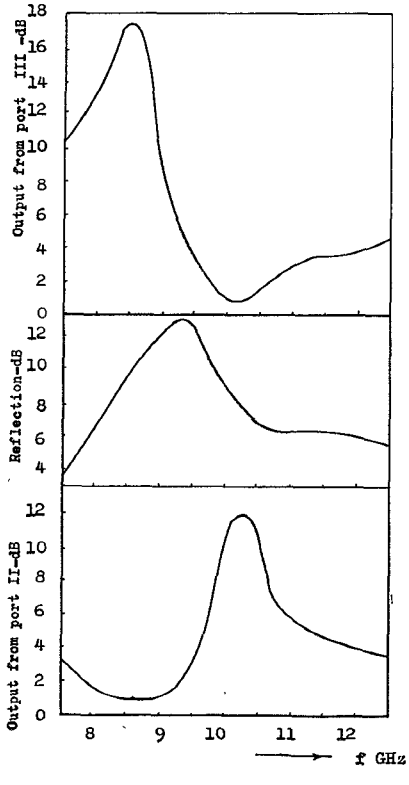

Fig. 15. Circulator characteristics for symmetrical T junction using sample TT1-109, $R=0.35$ cm and $H_{in}=200$ Oe.

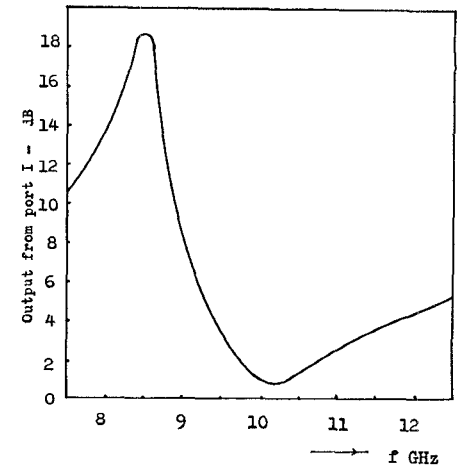

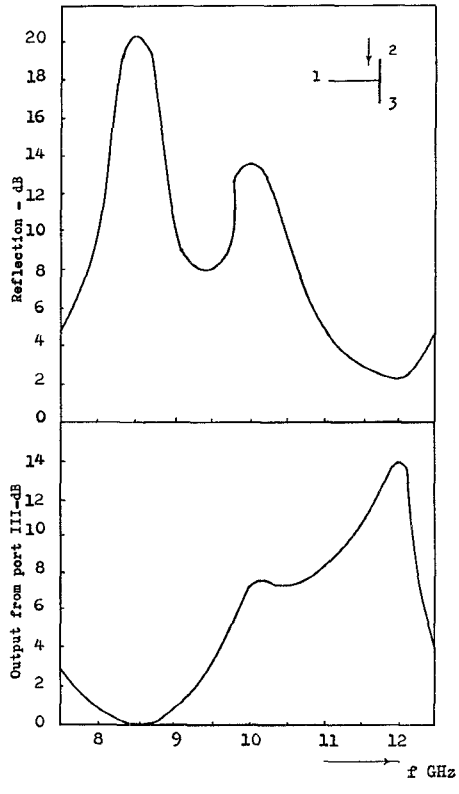

Fig. 16. Circulator characteristics for nonsymmetrical T junction (input from port 2) using sample TT1-109, $R=0.35$ cm and $H_{in}=200$ Oe.

Fig. 15, have the same general trends as with sample TT2-130.

2) Input from the Nonsymmetrical Arm (Port 2): In these calculations, the input signal is applied through port 2. The calculations for sample TT2-109 are shown in Fig. 16, with the value of the dc magnetic field 200 Oe as before.

Comparing this result with the corresponding result of the symmetrical case shown in Fig. 15; it is clear that circulation takes place for both cases at 8.5 GHz in the same direction. This circulation direction is opposite to that of the Y-junction circulator. At the circulation frequency (8.5 GHz) the performances obtained with the input applied to the nonsymmetrical port (port 2) are superior to applying the input to the symmetrical port, since the former has higher isolation and

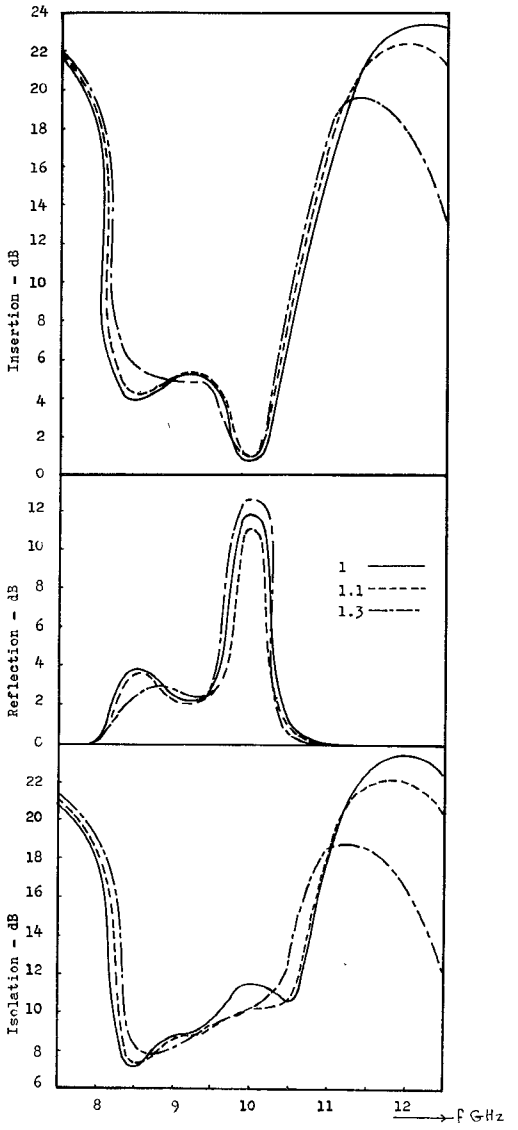

Fig. 17. Circulator characteristics for a Y-junction latching circulator using sample TT1-109, $R_3=0.35$ cm and $R_2/R_1=1$, 1.1, and 1.3.

lower reflection and insertion loss. Fig. 16 also shows that another circulation, in the opposite direction, occurs at around 10 GHz with inferior performance. It has the same direction and circulation frequency as the Y-junction circulator.

The characteristics of the T circulator lead to its use in the same applications as the Y circulator. In addition, other applications are also possible. As an example, when sample TT1-109 is used, and the junction is excited at 10 GHz from port 1 and at 8.5 GHz from port 2, the output is added at port 3. This property may be used in the design of mixers.

C. Latching Y-Junction Circulator

Numerical solutions are made in this case using the ferrite sample TT1-109. The external radius of the ferrite assembly is chosen to be 0.35 cm, which is the same as that used in the simple rod Y-junction circulator. The dielectric constant of the nonmagnetic gap is assumed to have the same value as the ferrite material. The characteristics of the latching circulator are obtained for three different values of the nonmagnetic gap width. In all the calculations the area of the ferrite post is taken equal to the area of the ferrite ring. Thus the gap width is determined by the ratio R_2/R_1 and the value of R_3. It is to be noted that no applied dc field is required in the latching circulator, hence the value of H_{in} is zero.

The limiting case of zero nonmagnetic gap ($R_2/R_1=1$) is shown in Fig. 17. Comparing this result with that of the simple ferrite-rod Y junction of Fig. 6, we see that both junctions have the same circulation frequency. However, the latching circulator has a degraded performance compared to the simple rod Y junction. There is almost a complete reflection at the upper and lower portions of the frequency band. The bandwidth is also reduced and this behavior is similar to the stripline latching circulator studied by Siekanowicz and Schilling [6]. This reduction in bandwidth is attributed to the opposite direction of dc magnetization in the inner and outer ferrite cylinders.

The effect of the gap width on the circulator performance is studied by repeating the calculations for two other values of R_2/R_1 which are 1.1 and 1.3, maintaining R_3 constant. These results are also shown in Fig. 17. It clearly indicates that only slight differences in the performance are observed in the studied range of R_2/R_1.

It is important to note that keeping the outer radius R_3 constant while increasing the ratio R_2/R_1, the volume of the ferrite decreases as $1/[1+(R_2/R_1)^2]$. This can be of value to reduce the dissipation loss once the dielectric-ring material is made less lossy than the ferrite material. Moreover, the switching energy which is proportional to the ferrite volume is reduced by increasing the ratio R_2/R_1.

V. Conclusion

The numerical results obtained for the symmetrical three port circulator characteristics are found to be in excellent agreement with the previously published experimental results of Davis and Castillo. The agreement includes the frequency of best isolation, the value of isolation at this frequency, and also the general shape of the reflection-coefficient characteristics, since it accounts for the double humps that exist in the experimental measurements. The power of this technique is further strengthened by the fact that it reveals information from which the electromagnetic-field components and the power-density distributions inside the junction are obtained.

To demonstrate the value of the adopted technique for a junction with less symmetry, the T junction is taken as an example. It is shown that two types of excitations are possible which are the symmetrical and nonsymmetrical excitations. In general it is found that the general shape of the characteristic curves depends on the port selected for excitation. Circulation is found to occur at two different frequencies in the two opposite directions of circulation. The performance of the junction is not the same at these two frequencies and depends on the ferrite sample properties used.

The obtained numerical results for the latching Y junction show that the performance is not affected by the variation of the gap width up to the calculated values (ratio $R_2/R_1=1.3$). In general it is found that the latching circulator has inferior performance compared with the unidirectional Y-junction circulator, which is the same result as obtained for the stripline latching circulator [6].

The method used in this paper could be applied to the study of the effect of the ferrite-rod dislocation from the junction axis. The dislocation may be intentional, as for example in the T junction, in order to seek the best possible performance unavoidable or due to manufacturing tolerances. The authors

intend to study this effect and other nonsymmetrical junctions in a future publication.

References

[1] J. B. Davies, "An analysis of the m-port symmetrical H-plane waveguide junction with central ferrite post," *IRE Trans. Microwave Theory Tech. (1962 Symposium Issue)*, vol. MTT-10, pp. 596–604, Nov. 1962.

[2] L. E. Davis and J. B. Castillo, Jr., "Computer-aided design of 3-port waveguide circulators," R&D Tech. Rep. ECOM-0491-F, Oct. 1968.

[3] J. B. Castillo, Jr., and L. E. Davis, "Computer-aided design of 3-port waveguide junction circulators," *IEEE Trans. Microwave Theory Tech.*, vol. MTT-18, pp. 25–34, Jan. 1970.

[4] L. Lewin and E. Nielsen, "On the inadequacy of discrete mode-matching techniques in some waveguide discontinuity problems," *IEEE Trans. Microwave Theory Tech.*, vol. MTT-18, pp. 364–372, July 1970.

[5] L. Lewin, "On the restricted validity of point-matching techniques," *IEEE Trans. Microwave Theory Tech. (1970 Symposium Issue)*, vol. MTT-18, pp. 1041–1047, Dec. 1970.

[6] W. W. Siekanowicz and W. A. Schilling, "A new type of latching switchable ferrite junction circulator," *IEEE Trans. Microwave Theory Tech.*, vol. MTT-16, pp. 177–183, Mar. 1968.

[7] H. Y. Yee and N. F. Audeh, "Uniform waveguides with arbitrary cross-section considered by the point-matching method," *IEEE Trans. Microwave Theory Tech. (1965 Symposium Issue)*, vol. MTT-13, pp. 847–851, Nov. 1965.

[8] J. A. Fuller and N. F. Audeh, "The point-matching solution of uniform nonsymmetric waveguides," *IEEE Trans. Microwave Theory Tech.* (Corresp.), vol. MTT-17, pp. 114–115, Feb. 1969.

[9] R. H. T. Bates, "The point-matching method for interior and exterior two-dimensional boundary value problems," *IEEE Trans. Microwave Theory Tech.* (Corresp.), vol. MTT-15, pp. 185–187, Mar. 1967.

[10] J. B. Castillo and L. E. Davis, "A higher order approximation for waveguide circulators," *IEEE Trans. Microwave Theory Tech.* (Short Paper), vol. MTT-20, pp. 410–412, June 1972.

Equivalent Circuit for Partially Dielectric-Filled Rectangular-Waveguide Junctions

C. T. M. CHANG

Abstract—**The problem of electromagnetic-wave propagation in junctions between two symmetrically, partially dielectric-filled waveguides was investigated, and the solution is presented in the form of a two-port equivalent circuit. This equivalent circuit includes an ideal 1:1 transformer, which is connected to transmission lines with impedances equal to those of the two waveguides, in cascade with a T network. Elements of the T network and the characteristic wave impedances of these partially dielectric-filled waveguides have been studied, and the results are presented in graphs for different dielectric constants, slab thicknesses, and operating frequencies.**

I. Introduction

IN RECENT YEARS there has been growing interest in waveguide sytems containing sections of partially dielectric-filled rectangular waveguides. Considerable literature has been devoted to the study of the different characteristics of partially dielectric-filled waveguides [1]–[10] and their applications to various microwave devices [11]–[15]. In many of these applications, the partially dielectric-filled waveguides are fed by empty waveguides and are sometimes terminated into another empty waveguide. Therefore, it is important that the characteristics of the junctions between the empty and partially dielectric-filled waveguide be studied so that some impedance-matching techniques [16] may be developed to minimize reflections at different locations along the waveguide system.

Earlier, several attempts [4], [17]–[19] were made to obtain the equivalent circuits for a number of empty to partially dielectric-filled rectangular-waveguide junctions employing various modified schemes of variational methods developed by Schwinger [20]. However, only a few crude calculations using simplified equivalent circuits were presented, and they were justified by comparing their results to reflection measurements. The reflection from a waveguide junction is caused by the change of the characteristic wave impedances across the junction, as well as the junction reactances, which are due to the stored energy in the nonpropagating modes at the junction. The reflections given in the examples in these earlier works were caused primarily by the former. Therefore, it becomes difficult to extract the small effect due to junction reactances from the experimental measurements and make an accurate comparison.

In the present work we report an investigation of dielectric-filled waveguide junctions in six different arrangements. It is found that despite their differences in geometries, they can all be represented by the equivalent circuit of Fig. 1(g). The effects of dielectric constants, thickness of dielectric slabs, and operating frequencies on various equivalent circuit parameters were studied and compared so that some general properties of these junctions could be understood.

Since this work is stimulated by the development of a microwave discharge chamber [21] that is partially dielectric filled and is operating in the dominant transverse electric (TE) mode,[1] present investigation is limited to junctions in-

Manuscript received September 7, 1972; revised January 26, 1973. This work was performed under the auspices of the U. S. Atomic Energy Commission.

The author is with the Argonne National Laboratory, Argonne, Ill. 60439.

[1] It should be noted that modes propagating inside a partially dielectric-filled waveguide are, in general, a mixture of regular TE and TM modes of the rectangular waveguide (see [1]).